

PHYSICS OF OUR DAYS

PACS number: 91.30.Px

Slow slip on tectonic faults

A.A. Ostapchuk

DOI: https://doi.org/10.3367/UFNe.2025.11.040061

Contents

Abstract. Slow slip is one of the mechanisms of relaxation of tectonic stresses in the Earth's crust. It has been recorded in seismically active zones all over the world, and it is accompanied by low-frequency and very low-frequency earthquakes. The paper presents modern concept about the physics of slow slip and examines the spatiotemporal links between slow slip and ordinary earthquakes. The discovery of slow slip phenomenon has revolutionized our understanding of the physics of deformation processes occurring in the Earth's crust and motivates us to develop a two-stage model of earthquake nucleation–initiation at the first stage of slow slip, which at the second stage transforms into rapid rupture.

Keywords: tectonic fault, slow earthquakes, asperity, frictional stability

1. Introduction. Essence of the discovery

The evolution of the Earth as a planet has been accompanied by energy exchange among different geospheres and by the occurrence of catastrophic natural phenomena. Large earthquakes originating in the Earth's lithosphere cause severe economic and societal damage. Identifying the mechanisms of earthquake nucleation and initiation remains a central problem in geophysics, seismology, and geology [1, 2].

Large tectonic faults divide the Earth's crust into geoblocks. Within these, smaller faults and fractures form boundaries of more localized and relatively stable regions. A 'fault' is defined as a zone of mechanical discontinuity in the geoenvironment — the boundaries of geoblocks that have undergone significant relative deformations. The discrete structure of the lithosphere and rocks is perhaps one of its fundamental properties [3, 4]. Driven by convective currents in the upper mantle, lithospheric plates (the largest geoblocks) slowly move relative to one another, determining the structure of the Earth's surface on timescales of millions of years and generating large earthquakes on timescales of tens and hundreds of years [5, 6].

In 1910, H.F. Reid, using data on the surface manifestations of the 1906 San Francisco earthquake, proposed that earthquakes are associated with tectonic faults in the Earth's crust [7]. Today, the spatial localization of seismicity cannot be explained without considering hierarchical interblock boundaries (plate boundaries, tectonic faults, and fractures) (Fig. 1).

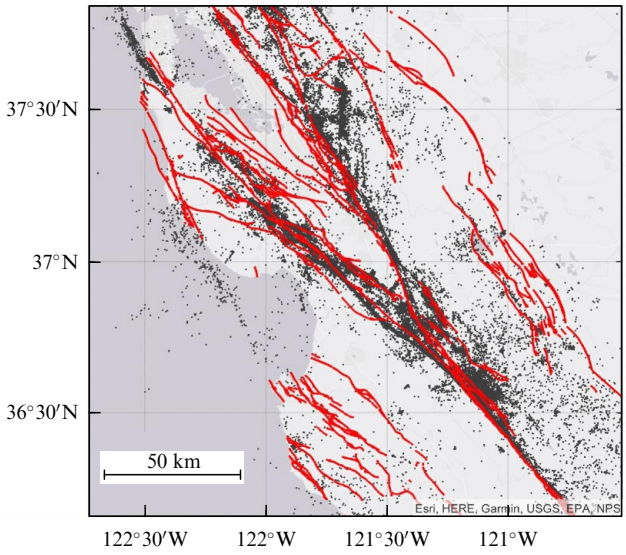

Figure 1. Comparison of seismicity maps and active tectonic faults in Northern California. Black dots indicate the epicenters of earthquakes recorded by the Northern California seismic network between January 1984 and December 2011. Red lines show active faults according to the U.S. Geological Survey.

A.A. Ostapchuk
(1) Sadovsky Institute of Geosphere Dynamics,
Russian Academy of Sciences,
Leninskii prosp. 38, korp. 1, 119334 Moscow, Russian Federation
(2) Moscow Institute of Physics and Technology
(National Research University),
Institutskii per. 9, 141701 Dolgoprudnyi, Moscow region,
Russian Federation
E-mail: ostapchuk.aa@idg.ras.ru

Received 14 July 2025, revised 6 November 2025
Uspekhi Fizicheskikh Nauk **196** (2) 173 – 181 (2026)
Translated by I.A. Ulitkin

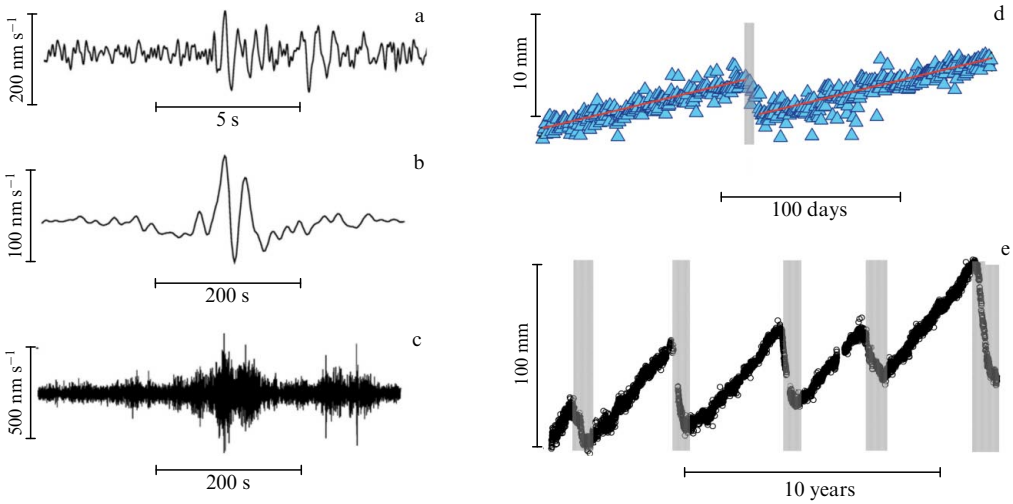

Figure 2. Examples of (a–c) seismic and (d, e) geodetic records of slow-slip events. (a) LFE earthquake, Japan [18]; (b) VLFE earthquake, Japan [19]; (c) tectonic tremor, Japan [18]; (d) SSE event, Cascadia, USA [14]; and (e) SSE event, Guerrero, Mexico [20].

The first experiments aimed at studying the behavior of geomaterials under high pressures showed that shear stress at the interface between rock blocks can either lead to plastic flow or dynamic rupture [8]. During a rupture, the medium in the contact zone disintegrates and blocks undergo relative displacement. Despite the impossibility of recreating deep PT conditions, it was assumed that the observed effects have much in common with processes occurring in real geological settings. In 1966, Brace and Byerlee [9] proposed that crustal earthquakes result from stick-slip along existing or newly formed faults (geoblock contacts) [9]. The seismic waves observed during this process correspond to the release of a portion of the elastic deformation energy accumulated in the geoblocks. According to the modern paradigm, most earthquakes are caused by frictional slip on pre-existing faults [10, 11].

For a long time, stresses accumulated in the Earth's crust are released either through earthquakes, with the 'instantaneous' disruption of geoblock contacts, or through continuous aseismic slip (creep) at a rate of several centimeters per year [12]. The picture began to change qualitatively with the advent of digital observation technologies and the improvement of measuring instruments. Deformation events were discovered with slip velocities several orders of magnitude higher than background ones, but significantly slower compared to the rupture propagation velocity during 'ordinary' earthquakes [13–15]. Dense networks of continuous geodetic and geophysical monitoring, the use of broadband high-sensitivity seismic stations made it possible to discover a new class of deformation events — slow slip on faults, which is a transitional stage from aseismic continuous creep to dynamic failure (associated with an ordinary earthquake) [16]. Slow-slip phenomena include low-frequency earthquakes (LFEs), very low-frequency earthquakes (VLFEs), nonvolcanic tremor, and long-period slow slip events (SSEs) detected geodetically (Fig. 2). Slow-slip phenomena are observed in all seismically active regions of the planet [17].

Slow-slip phenomena occur not only as an independent type of event, but can also be associated with other deformation processes, such as foreshocks [21], aftershocks [22, 23] and earthquake swarms [24]. Slow-slip phenomena can also be gravitational in nature, such as ice earthquakes [25] or landslide processes [26].

2. Description of slow-slip phenomena

The scale of slow-slip phenomena can be described in terms of the seismic moment [27]:

$$M_0 = GUS\,, \tag{1}$$

where G is the shear modulus of rock in the source, S is the source (rupture) area, and U is the relative displacement of the fault faces in the source. Generally speaking, the relative displacement of the fault faces is a complex function of space and time, and so its average value is used for estimation. The use of the seismic moment is justified by the fact that its magnitude is independent of the details of the process evolution in the source and is determined by the asymptotic behavior of the displacement spectrum in the low-frequency range. On the basis of the seismic moment, the earthquake moment magnitude M_w is determined from the relation [28]:

$$M_\mathrm{w} = \frac{2}{3}(\lg M_0 - 9.1)\,. \tag{2}$$

An important parameter describing the dynamics of the process development at the source is the rupture propagation velocity, which for slow-slip phenomena is determined from the relation:

$$V_\mathrm{r} = \frac{\Lambda}{T}\,, \tag{3}$$

where Λ is the characteristic rupture length and T is the slip duration. Duration is the parameter that is determined most reliably.

The parameters of slow-slip seismic events are appropriately compared with those characteristic of ordinary earthquakes [15]. For ordinary earthquakes, the rupture propagation velocity is $V_\mathrm{r} = 1.5 - 3$ km s^{-1}; the duration depends on the event magnitude and ranges from milliseconds to tens of seconds for the largest earthquakes. For LFE events, the rupture velocity is $V_\mathrm{r} = 50 - 1000$ m s^{-1}, and their duration is an order of magnitude longer than for ordinary earthquakes with the same seismic moment. Also, LFE events exhibit a significantly lower fault face displacement velocity, 0.01–0.1 m s^{-1} (compared to up to 5 m s^{-1} for ordinary

earthquakes). The VLFE events should be considered a subgroup of LFE events for which the rupture propagation velocity is $V_r = 10-100$ m s^{-1}; Moreover, during VLFE events, the main part of seismic energy is released in the frequency range of less than 1 Hz, while for LFEs the range is 1–10 Hz [29]. During LFE and VLFE events, the fraction of accumulated deformation energy spent on the emission of seismic vibrations is significantly less than during ordinary earthquakes [15]. Seismically detectable slow-slip phenomena lasting up to ~ 200 s can only be observed at low-noise stations located directly above the slow-slip zone [19]. Detection is based on an analysis of the dynamics of the process in time, described by the rate of changes in the seismic moment $dM_0(t)/dt$, which, under conditions of heterogeneity of the geoenvironment, is nonmonotonic and its variations are stochastic in nature [30].

Tremor, LFEs, and VLFEs can be recorded in a single seismic record. It is assumed that tremors represent a swarm of LFE events, while LFE and VLFE events can occur together [31]. For this reason, all these seismic events should be considered as different manifestations of a single process — *slow slip on a fault*. All these seismic events are collectively termed 'slow earthquakes.'

Geodetically detected SSE events are divided into events lasting 1–2 weeks and events lasting up to several years [32, 33]. For such events, the estimate of the rupture propagation velocity yields values of $V_r = 0.1-20$ km day^{-1}. On the basis of GNSS observations and tensometry data, SSE events with minimum magnitudes of $M_w = 5.3-5.7$ and duration $T = 1.5-2$ days can be reliably detected, while slow slip is practically not manifested in time series shorter than 10^5 s (~ 1 day) [34]. The implementation of SSE events is often accompanied by the initiation of swarms of slow earthquakes. Features of the activation of swarms of LFE events have been established in the Guerrero zone (Mexico) [35]. When displacement along the fault occurs at an extremely low velocity, LFEs are initiated independently of each other, and the flow of events appears Poissonian. When slow slip is initiated, clustering of LFE events begins to be observed in time. This dynamics of LFE event initiation is similar to the spatiotemporal evolution of the flow of ordinary earthquakes [36]. Studies conducted in the Nankai Trough (Japan) [37] made it possible to record the propagation of SSEs with a velocity of $V_r = 1-2$ km day^{-1}, accompanied by the migration of VLFE events.

The difference between ordinary earthquakes and slow-slip events is most clearly manifested in the diagram of the dependence of the event duration on its seismic moment (Fig. 3). For ordinary earthquakes, the energy similarity relations are satisfied, according to which both the linear dimensions of the source and the earthquake source time are proportional to the cube root of the seismic moment ($T \sim M_0^{1/3}$). At the same time, the set of data on slow-slip events demonstrates a linear dependence of the event duration on the seismic moment ($T \sim M_0$).

Although there is an observational gap between the slow slip events detected from seismological and geodetic observations, events that could fill the gap between the two regions of the diagram have been currently reported [40, 41]. Of particular interest among these are the events in the Izu-Bonin Trench region (Japan) [41]. After the $M_w6.0$ earthquake on September 1, 2015, two events were recorded that cannot be related to the aftershock process. The combined seismic moment of these two events is 17 times greater than

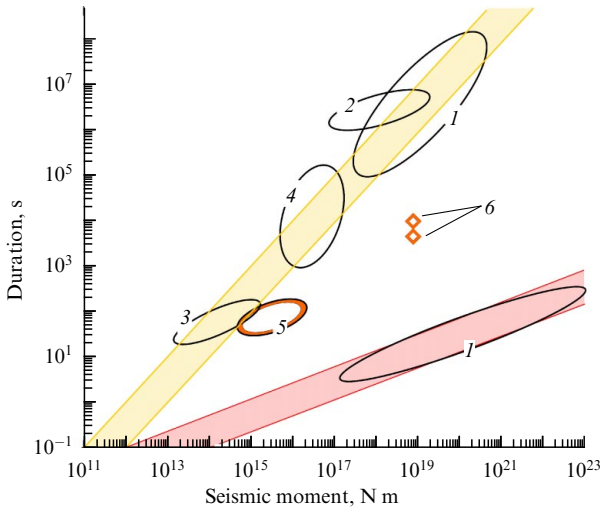

Figure 3. Duration of ordinary earthquakes and slow-slip events as a function of seismic moment. The red area shows the characteristic dependence for ordinary earthquakes; the yellow area, for slow-slip events. The ellipses denote the regions containing 95% of the events. The numbers refer to the following studies: (*1*) [15], (*2*) [38], (*3*) [19], (*4*) [39], (*5*) [40], and (*6*) [41].

the seismic moment of the $M_w6.0$ earthquake. The first event was recorded immediately after the earthquake, its duration was 153 min, and the rupture propagation velocity was $V_r = 2-3$ m s^{-1}. The second event, with a duration of 73 min and $V_r = 5-7$ m s^{-1}, occurred 3 days after the $M_w6.0$ earthquake. Recording events in the Izu-Bonin Trench became possible after a network of absolute pressure sensors on the ocean floor at a depth of 5 km, which increased monitoring sensitivity.

3. Physical mechanism for slow slip

If a tectonic fault or fracture form in a rock mass, the main deformation localizes at these discontinuities. The dynamics of fault deformation is largely determined by the properties of the constituent rocks. Systematization of research results has shown that both the strength and frictional properties of rocks can vary significantly. In earthquake focal zones, rocks are characterized by high frictional strength, corresponding to Byerlee's law [42]:

$$\tau_p = \begin{cases} 0.85\sigma_N, & \sigma_N < 2 \text{ kbar}, \\ 0.5 + 0.6\sigma_N, & \sigma_N > 2 \text{ kbar}. \end{cases} \quad (4)$$

At the same time, some rocks are characterized by extremely low strength, corresponding to friction coefficients of 0.1–0.3 [43]. Along with frictional strength, frictional stability is an important property that governs the dynamics of slip on faults. The Rate&State friction law is widely used to describe the behavior of rocks [44, 45]:

$$\mu = \left(\frac{\tau}{\sigma_N}\right) = \mu_0 - a\ln\left(\frac{V_0}{V}\right) + b\ln\left(\frac{V_0\theta}{D_c}\right),$$
$$\dot{\theta} = 1 - \left(\frac{V\theta}{D_c}\right), \quad (5)$$

where μ_0 is the friction coefficient corresponding to stable slip at a velocity V_0; a, b, and D_c are empirical constants; θ is the state variable; and V is the slip velocity. In a steady state,

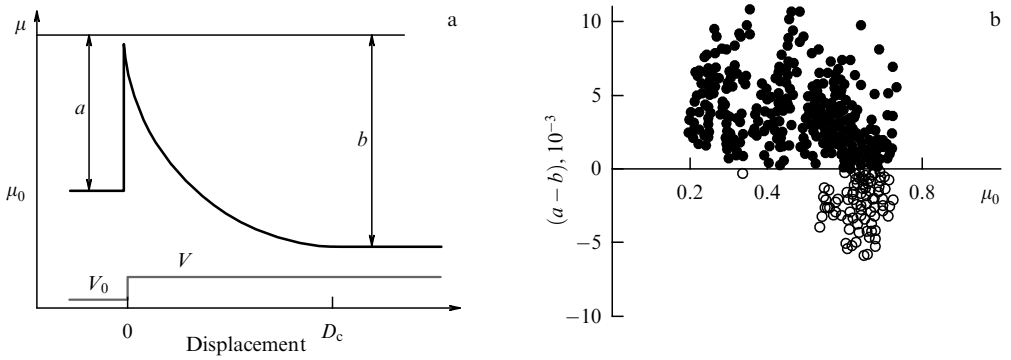

Figure 4. Frictional stability of rocks. (a) Variation of the friction coefficient with slip velocity for rocks exhibiting velocity-weakening behavior (μ_0, a, b, D_c are the Rate&State friction law parameters). The slip velocity increases sharply from V_0 to V at the moment of displacement onset '0;' (b) dependence of the friction parameter (a–b) on the friction coefficient [2].

when $\dot{\theta} = 0$, the change in the friction coefficient is given by the expression

$$\mu(V) = \mu_0 + (a - b) \ln \left(\frac{V}{V_0} \right). \qquad (6)$$

It can be seen that the quantity (a–b) is a critical parameter that controls frictional behavior. A typical change in the friction coefficient with changing slip velocity is shown in Fig. 4.

For $(a-b) < 0$, rocks exhibit velocity-weakening behavior: with increasing slip velocity, the friction coefficient becomes less than its initial value at displacements greater than the critical value D_c. For $(a-b) > 0$, rocks exhibit velocity-strengthening behavior: with increasing slip velocity, the friction coefficient becomes higher than its initial value. If a rock exhibits velocity-strengthening properties, the fault is stable; velocity-weakening behavior promotes the development of dynamic instability. For rocks, a relationship has been observed between the friction coefficient μ_0 and the friction parameter $(a-b)$ (Fig. 4b). Rocks with a low friction coefficient exhibit velocity strengthening, while rocks with a high friction coefficient exhibit both velocity strengthening and weakening. The frictional stability of rocks with a high friction coefficient depends significantly on the loading rate, shear amplitude, and PT conditions [46, 47].

Figure 5 illustrates a depth-dependent model of fault properties, which explains the conditions for the formation of different slip regimes and is consistent with geological and seismological observations [10, 48]. Within the model, regions with velocity-strengthening behavior form at shallow and great depths. At shallow depths, this behavior is associated with the presence of decompressed granular material, whereas at great depths, it is related to the transition to plastic deformation at high temperatures. In such areas, faults are stable and exhibit stable creep. With increasing depth, the geomaterial consolidates, and the rocks exhibit rapid weakening, which causes ordinary earthquakes in this zone.

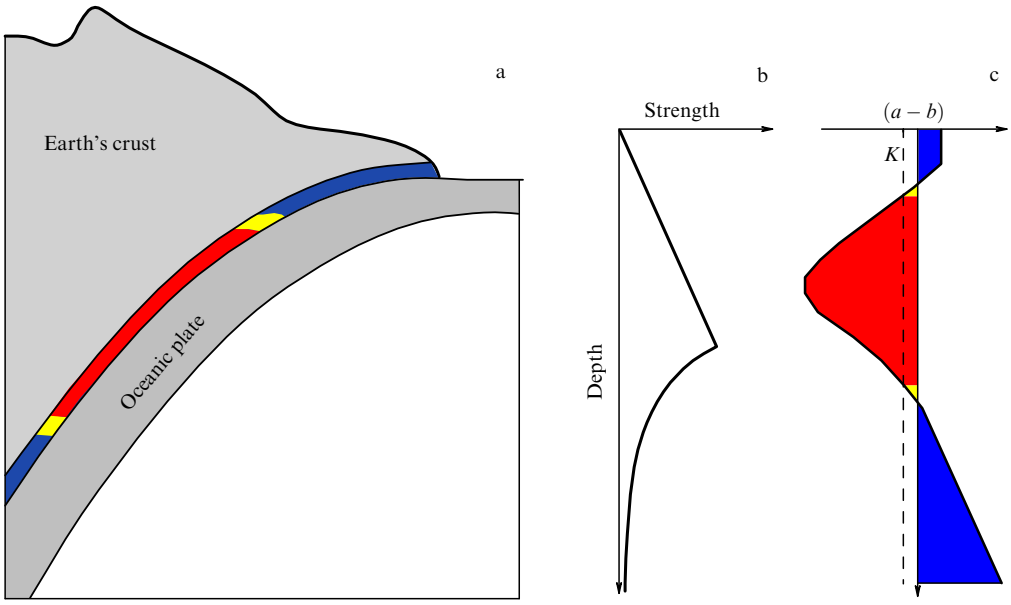

Figure 5. Variation of the frictional properties of fault-forming rocks with depth (red, region of velocity-weakening behavior; yellow, conditionally stable region; and blue, velocity-strengthening behavior). (a) Zones of localization of different slip regimes illustrated using the example of a subduction zone; (b) variation of rock strength with depth; (c) variation of the friction parameter with depth. The dashed line corresponds to the critical value of rheological stiffness at which the fault becomes dynamically unstable.

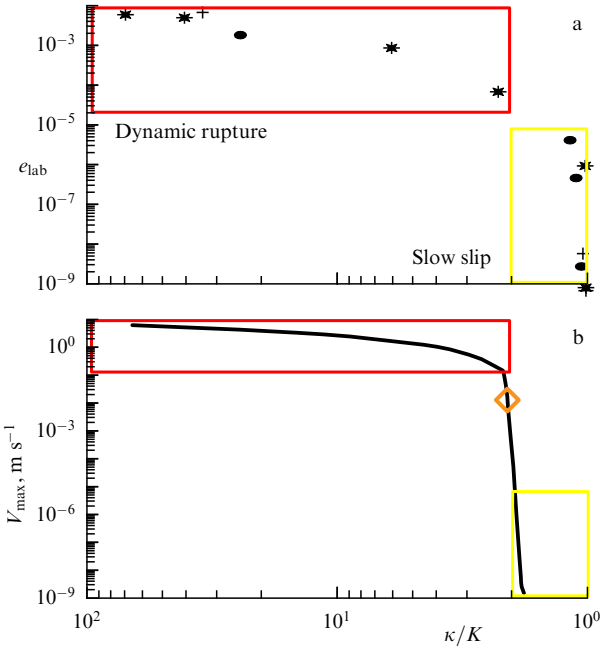

Figure 6. Variation of the parameters characterizing different slip regimes as a function of the ratio of the rheological stiffness to the host-rock stiffness (κ/K). (a) Variation of the reduced radiated energy in laboratory experiments [50]; (b) variation of the maximum fault slip velocity in numerical experiments [49]. The diamond indicates the parameters of events recorded in the Izu-Bonin Trench [41].

For earthquakes to initiate, the rate of dynamic release of elastic deformation energy must be no less than the specific energy of rupture propagation. Under conditions of frictional slip along the contact of geoblocks, this means that the stiffness of host rock (K) must be lower than the rheological stiffness of the fault (κ). In terms of the Rate&State friction law, this condition can be written as

$$\frac{\kappa}{K} = \frac{-\sigma(a-b)/D_c}{G/\Lambda} = \frac{-\sigma(a-b)}{G}\,\frac{\Lambda}{D_c} > 1\,. \qquad (7)$$

In relatively stable zones ($0 < \kappa/K < 1$), instability can develop under dynamic stress disturbances [10]. Slow-slip zones are regions of transition from dynamic stability to dynamic instability. Numerical and laboratory experiments show that the transition from dynamic failure to stable creep occurs at $1 < \kappa/K < 2$ (Fig. 6) [49, 50]. The diagram of the fault displacement velocity versus the stiffness ratio exhibits a discontinuity between regions characteristic of slow-slip phenomena and ordinary earthquakes. Notably, the above-described events in the Izu-Bonin Trench region [41] fall precisely within the discontinuity region of the diagram.

In general, interblock contact is characterized by strong spatial heterogeneity in the distribution of frictional properties [23, 43, 51] (Fig. 7). In the fault slip plane, so-called asperities are formed. These asperities are composed of rocks with a high friction coefficient and are likely to exhibit velocity-weakening behavior. These asperities are separated by dynamically stable zones — barriers — characterized by low friction coefficients and velocity-strengthening behavior. The configuration of these asperities and their rheological properties determine the slip regimes along a local section of the fault.

A small change in the rheological properties of the barrier zones can lead to a radical change in the slip regime on the fault (Fig. 7b) [52]. If the friction parameter $(a-b)$ exceeds a critical value, isolated ruptures develop at individual asperities; if $(a-b)$ is below the critical value, the rupture propagates across the entire fault (interblock contact) area. Initiated at one asperity, the rupture propagates in both directions. In the barrier zones, the slip velocity decreases sharply and then increases again at adjacent asperities [53]. Thus, the complex spatial configuration of asperities and the spatial heterogeneity of the frictional properties of the interblock fault contact can give rise to complex slip dynamics.

4. Link of slow slip to earthquakes

4.1 Slow slip after earthquakes

Slow slip is also associated with the evolution of ordinary earthquake sources. Slow postseismic slip is regularly observed after large earthquakes. Postseismic slip can be interpreted as the response of areas with velocity-strengthening behavior around asperity ruptures to a sudden stress change caused by the earthquake [54]. A sharp stress jump leads to an almost instantaneous increase in slip velocity in

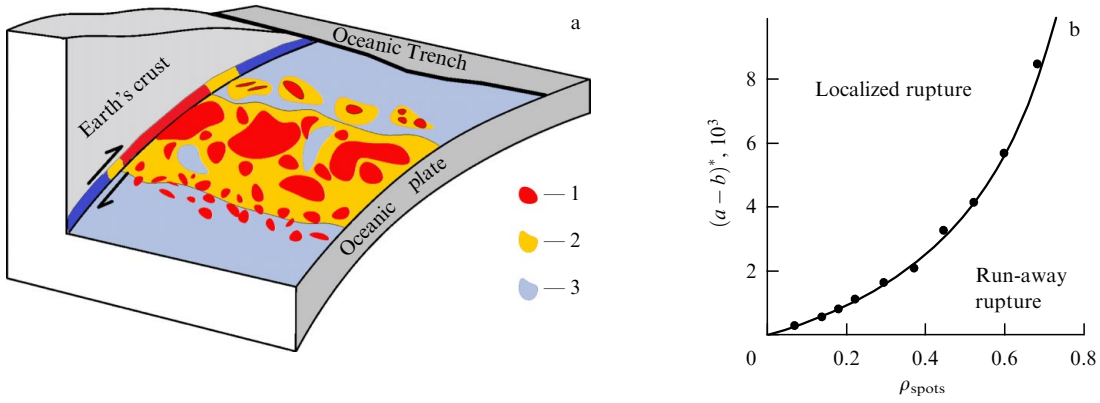

Figure 7. Distribution of frictional properties over the interblock contact (using a subduction zone as an example). (a) Structural model of a subduction zone ((*1*) asperities, (*2*) conditionally stable zone, and (*3*) dynamically stable zone). Colors correspond to Fig. 5; (b) dependence of the critical value of the barrier friction parameter $(a–b)^*$, at which rupture propagates along the entire fault plane, on the density of asperities. Dots represent the results of numerical simulations [52].

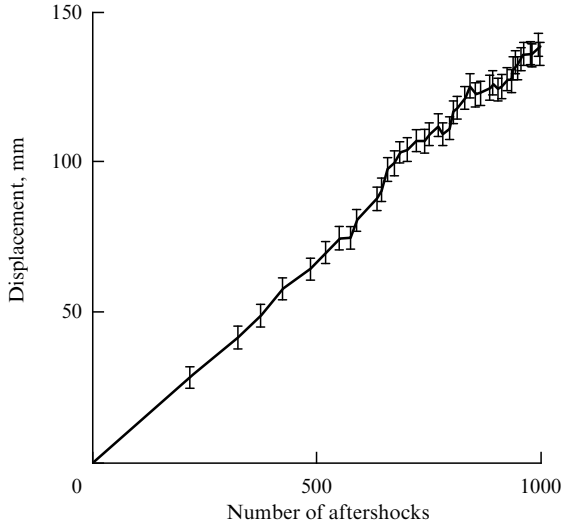

Figure 8. Comparison of the postseismic slip amplitude and the number of aftershocks following the $M_w8.3$ earthquake on September 16, 2015, in Illapela, Chile [57]. The surface displacement derived from GNSS observations at the PFRJ station and the number of aftershocks initiated within the fault segment located in the vicinity of the PFRJ station are shown.

the relatively stable regions surrounding the rupture, thereby initiating slow slip. The postseismic displacement U_{aft} depends on time according to a logarithmic law [54, 55]:

$$U_{\text{aft}}(t) = V_{\text{seis}} t_{\text{aft}} \ln\left(1 + \frac{t}{t_{\text{aft}}}\right), \tag{8}$$

where V_{seis} is the initial velocity of postseismic slip, and t_{aft} is the slip time constant. The duration of postseismic slip, depending on earthquake magnitude, ranges from several days to several years.

Analysis of the patterns of aftershock localization in the fault slip plane shows that aftershocks are clearly localized near the boundary of the earthquake source, occupying an increasingly larger area with time [23, 56]. A comparison of geodetic and seismological data on major earthquakes demonstrates a linear relationship between the amplitude of postseismic slip and the cumulative number of aftershocks (Fig. 8) [57].

According to current understanding, the aftershock sources of ordinary earthquakes correspond to ruptures of asperities located around the source of the main earthquake. Ruptures at smaller hierarchical scales are triggered by quasi-static and dynamic changes in the stress–strain field induced by the mainshock. Consequently, aftershock activity (the number of aftershocks per unit time) will depend on the density of the asperities. Assuming that the source of the main earthquake is a circular rupture [58], the aftershock activity initiated by postseismic slip can be expressed as

$$n(t) = \rho\big(W_{\text{aft}}(t)\big)\,\mathrm{d}A = \rho\big(W_{\text{aft}}(t)\big) 2\pi W_{\text{aft}}(t)\dot{W}(t)\,, \tag{9}$$

where ρ is the density of asperities, $\mathrm{d}A$ is the change in the area of the postseismic slip zone due to its propagation, and $W(t)$ is the distance from the source boundary to the slow-slip front ($\dot{W}(t) \sim \dot{U}_{\text{aft}}(t)$). Based on analyses of the relative positions of earthquake hypocenters within tectonic contact zones [59], it can be assumed that the density of asperities decreases with distance from the boundary inversely proportional to the distance ($\rho(W) \sim 1/W$). Then, the aftershock activity and the cumulative number of initiated aftershocks will have the form

$$n(t) \sim \frac{1}{1 + (t/t_{\text{aft}})}\,,$$
$$N(t) = \int n(t)\,\mathrm{d}t \sim \int \dot{W}(t)\,\mathrm{d}t \sim W(t)\,, \tag{10}$$

which is consistent with the well-known Omori law [60] and with the results of a comparison of geodetic and seismological data [57, 61]. This suggests that one of the physical mechanisms of aftershocks is the rupture of asperities triggered by the propagation of slow postseismic slip.

4.2 Slow slip before large earthquakes

The process of earthquake initiation is difficult to observe instrumentally. Most existing earthquake source models were developed based on concepts involving the formation and evolution of either a single fracture or a fracture network (the dilatant-diffusion model [62], the avalanche-unstable fracture model [63], and the medium consolidation model [64]). Advances in understanding fault structure and slip regimes have shown that earthquakes are essentially rapid frictional slip events is mediated by rupture propagation and the evolution of frictional contact along interfaces between rock blocks.

With the development of geodetic and seismic monitoring networks, potential indicators of short-term activation of slip on asperities — the precursors of large earthquakes — have been recorded [21, 65, 66]. Based on GNSS observations, Bletery and Nocquet [67] showed that earthquakes with $M_w > 7$ are preceded by a slow-slip phase lasting approximately 2 h prior to rupture. A two-stage rupture nucleation process at a single asperity is clearly observed in laboratory experiments: slow, steady slip initiates once a critical shear stress is reached; as the slow slip approaches the asperity boundary, a topological transition occurs, during which it smoothly transforms into a dynamic rupture [68–70].

Analysis of the source configuration of large earthquakes shows that most events ($\sim 73\%$) follow a single-asperity scenario. Earthquake sources with two or more asperities account for 27% of cases, with configurations involving both closely and widely spaced asperities [71]. The development of large-scale experimental setups in recent years has enabled detailed studies of the spatiotemporal evolution of slip on a model fault with a spatially heterogeneous structure [71–74]. In such experiments, the fault is modeled as a contact between the surfaces of meter-scale rock blocks; under applied normal and shear stresses, the blocks slide relative to each other (Fig. 9).

Experiments [71] demonstrate that when several asperities (zones of increased frictional strength exhibiting rapid weakening behavior) are formed at a fault boundary, rupture develops according to several scenarios determined by the relative positions of the asperities. When the distances between asperities are less than half their size (closely spaced asperities), rupture develops locally at one of the asperities and slow slip is initiated in the first stage. When the second asperity fails, rupture propagates across the entire fault surface, leading to rapid slip.

The development of a slow-slip zone in the vicinity of the source of an impending earthquake is clearly visible prior to the $M_w8.1$ earthquake that occurred on April 1, 2014, in

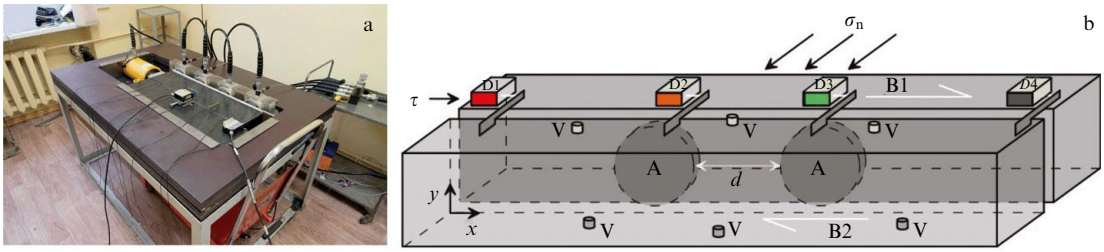

Figure 9. RAMA experimental setup for studying frictional slip on model faults with a spatially heterogeneous structure [71]. (a) General view of the setup; (b) scheme of the setup: (B1, B2) sliding and fixed blocks; (A) asperities characterized by increased strength and high-velocity-weakening behavior; (*d*) distance between asperities; (D1–D4) laser displacement sensors measuring relative block displacement; (V) acoustic emission sensors.

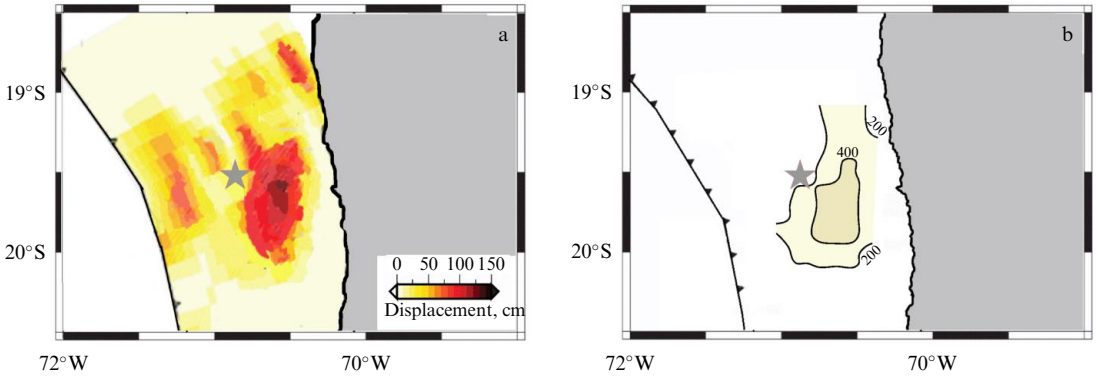

Figure 10. Displacement field associated with the M_w8.1 earthquake on April 1, 2014, in Iquique, Chile. The epicenter of the earthquake is marked by the star [75]. (a) Amplitude of displacement accumulated during slow slip from March 10 to March 31, 2014; (b) coseismic displacement at the mainshock source. Isolines corresponding to 200 cm and 400 cm are shown.

Iquique, Chile [75]. Seventeen days before the mainshock, all thirteen GNSS monitoring stations located along the coastline recorded slowly increasing westward motion, deviating from the typical interseismic eastward motion. The slow-slip displacement field calculated using the Okada model [76] is shown in Fig. 10a. The slow slip was localized over an area of 70 by 20 km, with a seismic moment of 4.4×10^{19} N m^{-1}, which corresponds to a moment magnitude of M_w7.0. The mainshock began with a small tremor, the epicenter of which was located outside the slow-slip zone. The maximum rate of seismic moment release during rupture occurred approximately 30 s after rupture initiation, with the rupture encompassing a large zone, including a slow-slip zone (Fig. 10b).

Slow slip before strong earthquakes can either represent an integral component of the nucleating dynamic rupture at a single asperity or occur as an independent event governed by the evolution of a fault with a complex asperity configuration. It is also important to note cases of seismogenic-aseismic deformation processes, where ordinary earthquakes alternate with slow-slip events without a clearly defined mainshock [41, 77].

5. Conclusions

This review demonstrates that slow slip is an important component of deformation processes in tectonic fault zones. A comprehensive understanding of such phenomena at various time intervals of the seismic cycle can be achieved through continuous long-term seismic and geodetic monitoring. Monitoring should take into account the geological and tectonic characteristics of the regions and changes in the hydrogeological regime. Such an approach will provide critical information for developing a unified model of tectonic fault deformation.

The physical mechanism underlying the formation of different slip regimes involves a topological transition from dynamic shear to slow slip within a narrow region of phase space. Identifying the geological and geophysical conditions under which this topological transition occurs is essential for developing a physical model of an earthquake source.

In conclusion, it is important to highlight three key areas in which knowledge of slow slip phenomena is critical:

- slow slip and slow earthquakes should be incorporated into statistical models used for seismic hazard assessment;
- models of strong earthquake sources developing along faults with heterogeneous spatial structure must take into account various stress relaxation scenarios;
- advancement of short-term earthquake forecasting requires the identification of reliable seismic and geophysical indicators of slow slip and its transformation into a dynamic rupture.

Acknowledgments. This work was supported by the Russian Science Foundation (Project No. 22-17-00204, Geomechanics of Crustal Faults — from Regional Scales to Microraptures Program).

References

1. Tikhotskii S A *Vestn. Ross. Akad. Nauk* **94** (10) 873 (2024) DOI:10.31857/S0869587324100016
2. Kocharyan G G *Izv. Phys. Solid Earth* **57** 439 (2021); *Fiz. Zemli* (4) 3 (2021)
3. Sadovskii M A *Dokl. Akad. Nauk SSSR* **247** 829 (1979)
4. Kocharyan G G *Dinamich. Protsessy Geosferakh* **16** (3) 23 (2024)

5. Keylis-Borok V I, Malinovskaya L N *J. Geophys. Res.* **69** 3019 (1964)
6. Fedotov S A, Solomatin A V *J. Volcanolog. Seismol.* **13** 349 (2019); *Vulkanolog. Seismolog.* (6) 6 (2019)
7. Reid H F *The Mechanics of the Earthquake. The California Earthquake of April 18, 1906. Report of the State Earthquake Investigation Commission. Report of State Investigation Commission* Vol. 2 (Washington, DC: Carnegie Institute of Washington, 1910)
8. Bridgman P W *J. Geology* **44** 653 (1936)
9. Brace W F, Byerlee J D *Science* **153** 990 (1966)
10. Scholz C H *Nature* **391** 37 (1998)
11. Kocharyan G G *Geomekhanika Razlomov* (Geomechanics of Faults) (Moscow: GEOS, 2016)
12. Kasahara K *Mekhanika Zemletryasenii* (Moscow: Mir, 1985); Translated from English: *Earthquake Mechanics* (Cambridge: Cambridge Univ. Press, 1981)
13. Kanamori H, Hauksson E *Bull. Seismolog. Soc. Am.* **82** 2087 (1992) DOI:10.1785/BSSA0820052087
14. Dragert H, Wang K, James T S *Science* **292** 1525 (2001)
15. Kocharyan G G et al. *Geodynamics Tectonophysics* **5** (4) 863 (2014)
16. Peng Z, Gomberg J *Nature Geosci.* **3** 599 (2010)
17. Schwartz S Y, Rokosky J M *Rev. Geophys.* **45** RG3004 (2007) DOI:10.1029/2006RG000208
18. Shelly D R, Beroza G C, Ide S *Nature* **446** 305 (2007)
19. Ide S et al. *Geophys. Res. Lett.* **35** L10305 (2008) DOI:10.1029/2008GL034014
20. Radiguet M et al. *Nature Geosci.* **9** 829 (2016)
21. Wang K et al. *J. Geophys. Res. Solid Earth* **129** e2023JB027209 (2024) DOI:10.1029/2023JB027209
22. Rolandone F et al. *Sci. Adv.* **4** eaao6596 (2018)
23. Ostapchuk A A *Dokl. Earth Sci.* **523** 31 (2025) DOI:10.1134/S1028334X25605899; *Dokl. Ross. Akad. Nauk. Nauki o Zemle* **523** 298 (2025)
24. Lohman R B, McGuire J J *J. Geophys. Res.* **112** B04405 (2007) DOI:10.1029/2006JB004596
25. Wiens D A et al. *Nature* **453** 770 (2008)
26. Psakhie S G et al. *Tribology Int.* **40** 995 (2007)
27. Aki K *J. Geophys. Res.* **72** 1217 (1967)
28. Hanks T C, Kanamori H *J. Geophys. Res.* **84** (B5) 2348 (1979)
29. Wei X et al. *Geophys. Res. Lett.* **51** e2023GL107988 (2024) DOI:10.1029/2023GL107988
30. Ide S, Yabe S *Pure Appl. Geophys.* **176** 1021 (2019)
31. Beroza G C, Ide S *Annu. Rev. Earth Planet. Sci.* **39** 271 (2011)
32. Nishikawa T, Ide S, Nishimura T *Prog. Earth Planet. Sci.* **10** 1 (2023)
33. Wallace L M et al. *J. Geophys. Res.* **117** B11402 (2012) DOI:10.1029/2012JB009489
34. Ide S, Beroza G C *Proc. Natl. Acad. Sci. USA* **120** e2222102120 (2023) DOI:0.1073/pnas.2222102120
35. Frank W B et al. *Sci. Adv.* **2** e1501616 (2016)
36. Zaliapin I et al. *Phys. Rev. Lett.* **101** 018501 (2008)
37. Edgington J R, Saffer D M, Williams C A *Science* **388** 1396 (2025)
38. Michel S, Gualandi A, Avouac J-P *Nature* **574** 522 (2019)
39. Bletery Q et al. *Earth Planet. Sci. Lett.* **463** 212 (2017)
40. Sugioka H et al. *Nature Geosci.* **5** 414 (2012)
41. Fukao Y et al. *J. Geophys. Res. Solid Earth* **126** e2021JB022132 (2021) DOI:10.1029/2021JB022132
42. Byerlee J *Pure Appl. Geophys.* **116** 615 (1978)
43. Collettini C et al. *Earth Planet. Sci. Lett.* **519** 245 (2019)
44. Dieterich J H *J. Geophys. Res.* **84** (B5) 2161 (1979)
45. Rice J R, Ruina A L *J. Appl. Mech.* **50** 343 (1983)
46. Collettini C et al. *Nature* **462** 907 (2009)
47. Verberne B A et al. *J. Geophys. Res. Solid Earth* **120** 8169 (2015)
48. Obara K, Kato A *Science* **353** 253 (2016)
49. Barbot S *Tectonophysics* **768** 228171 (2019)
50. Kocharyan G G et al. *Geophys. J. Int.* **208** (1) 521 (2017)
51. Fagereng A, Beall A *Philos. Trans. R. Soc. A* **379** 20190421 (2021)
52. Dublanchet P, Bernard P, Favreau P *J. Geophys. Res. Solid Earth* **118** 2225 (2013)
53. Kocharyan G G, Ostapchuk A A, Pavlov D V, in *Multiscale Biomechanics and Tribology of Inorganic and Organic Systems. In memory of Professor Sergey Psakhie* (Springer Tracts in Mechanical Engineering, Eds G-P Ostermeyer et al.) (Cham: Springer, 2021) p. 323, DOI:10.1007/978-3-030-60124-9_15
54. Perfettini H, Avouac J-P *J. Geophys. Res.* **109** B02304 (2004) DOI:10.1029/2003JB002488
55. Kocharyan G G, Kulyukin A A, Pavlov D V *Russ. Geology Geophys.* **47** 669 (2006); *Geologiya Geofiz.* **47** (5) 669 (2006)
56. Chalumeau C et al. *Nature* **628** 558 (2024)
57. Frank W B, Poli P, Perfettini H *Geophys. Res. Lett.* **44** 5374 (2017)
58. Brune J N *J. Geophys. Res.* **75** 4997 (1970)
59. Kocharyan G G, Ostapchuk A A *Phys. Mesomech.* **26** 82 (2023); *Fiz. Mezomekh.* **25** (5) 94 (2022)
60. Omori F *J. College Sci. Imperial Univ. Tokyo* **7** 111 (1894)
61. Perfettini H, Avouac J-P, Ruegg J-C *J. Geophys. Res.* **110** B09404 (2005) DOI:10.1029/2004JB003522
62. Scholz C H et al. *Science* **181** 803 (1973)
63. Myachkin V I et al., in *Fizika Ochaga Zemletryaseniya* (Physica of the Earthquake Source) (Trudy Inst. Fiziki Zemli im. O Yu Shmidta, Exec. Ed. M A Sadovskii) (Moscow: Nauka, 1975) p. 6
64. Dobrovol'skii I P *Teoriya Podgotovki Tektonicheskogo Zemletryaseniya* (Theory of Preparation of a Tectonic Earthquake) (Moscow: Inst. Fiziki Zemli im. O Yu Shmidta, 1991)
65. Trugman D T, Ross Z E *Geophys. Res. Lett.* **46** 8772 (2019)
66. Martínez-Garzón P, Poli P *Commun. Earth Environ.* **5** 120 (2024)
67. Bletery Q, Nocquet J-M *Science* **381** 297 (2023)
68. Latour S et al. *Geophys. Res. Lett.* **40** 5064 (2013)
69. Yamashita F et al. *Tectonophysics* **733** 193 (2018)
70. Gvirtzman S et al. *Nature* **637** 369 (2025)
71. Kocharyan G G et al. *Izv. Phys. Solid Earth* **61** 691 (2025); *Fiz. Zemli* (4) 199 (2025)
72. Mastella G et al. *J. Geophys. Res. Solid Earth* **127** e2021JB022789 (2022) DOI:10.1029/2021JB022789
73. Gridin G A et al. *Izv. Phys. Solid Earth* **59** 460 (2023); *Fiz. Zemli* (3) 139 (2023)
74. Yamashita F et al. *Tectonophysics* **733** 193 (2018)
75. Ruiz S et al. *Science* **345** 1165 (2014)
76. Okada Y *Bull. Seismolog. Soc. Am.* **75** 1135 (1985)
77. Villegas-Lanza J C et al. *Nature Geosci.* **9** 150 (2016)